Turk Neurosurg 35(6):936-942, 2025
DOI: 10.5137/1019-5149.JTN.48541-25.3

Original Investigation

Pediatrics

Received: 29.01.2025
Accepted: 29.04.2025
Published Online: 30.10.2025

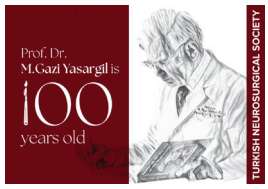

Cranial Aperture of the Optic Canal in Chiari Malformation Type 2: A Morphometric Study on CT Images

Mehmet Zeki ERDEM[1], Abdulmutalip KARAASLANLI[2], Abdulaziz YALINKILIC[1], Ozkan ARABACI[2], Zulkuf AKDEMIR[3], Burhan BEGER[4], Baris ASLANOGLU[5], Turan KOC[6], Orhan BEGER[7]

[1]Van Yüzüncü Yıl University, Faculty of Medicine, Department of Otorhinolaryngology, Van, Türkiye
[2]Van Yüzüncü Yıl University, Faculty of Medicine, Department of Neurosurgery, Van, Türkiye
[3]Van Yüzüncü Yıl University, Faculty of Medicine, Department of Radiology, Van, Türkiye
[4]Van Yüzüncü Yıl University, Faculty of Medicine, Department of Pediatric Surgery, Van, Türkiye
[5]Health Sciences University, Gazi Yaşargil Training and Research Hospital, Department of Neurosurgery, Diyarbakır, Türkiye
[6]Kahramanmaraş Sütçü İmam University, Faculty of Medicine, Department of Anatomy, Kahramanmaraş, Türkiye
[7]Gaziantep University, Faculty of Medicine, Department of Anatomy, Gaziantep, Türkiye

Corresponding author: Mehmet Zeki ERDEM ✉ mzekierdem1983@gmail.com

ABSTRACT

AIM: To identify morphological differences in the cranial aperture (CA) of the optic canal (OC) in patients with Chiari malformation type 2 (CMT2) by comparing them with healthy individuals.

MATERIAL and METHODS: Computed tomography images were analyzed for 40 patients with CMT2 (16 females, 24 males; mean age, 10.05 ± 4.51 years; age range, 6–18 years) and 40 control subjects (21 females, 19 males; mean age, 10.03 ± 4.81 years; age range, 6–18 years). Measurements included the height (HCA), width (WCA), and surface area (ACA) of the CA, as well as the distances from the CA to the anterior border of the anterior cranial fossa (AB-CA), lateral border (LB-CA), and midsagittal line (MSL-CA). Additionally, the angles of the OC were assessed in both the axial (APA) and sagittal planes (SPA).

RESULTS: In the CMT2 group, mean values were as follows: HCA 3.64 ± 0.81 mm, WCA 3.08 ± 0.87 mm, ACA 7.58 ± 2.84 mm^2, AB-CA 44.99 ± 7.69 mm, LB-CA 29.17 ± 5.03 mm, MSL-CA 7.07 ± 2.44 mm, APA 30.64° ± 6.03°, and SPA 24.31° ± 5.09°. In the control group, corresponding values were HCA 4.22 ± 0.60 mm, WCA 4.54 ± 1.04 mm, ACA 12.81 ± 3.80 mm^2, AB-CA 52.73 ± 6.71 mm, LB-CA 35.86 ± 4.33 mm, MSL-CA 10.21 ± 2.21 mm, APA 35.96° ± 3.23°, and SPA 28.64° ± 4.34°. All measurements were significantly smaller in the CMT2 group compared to controls ($p<0.001$).

CONCLUSION: Patients with CMT2 exhibit significantly reduced CA dimensions and angular measurements of the OC. These differences, particularly in depth and orientation, may be clinically relevant when planning surgical interventions such as OC decompression.

KEYWORDS: Chiari malformation type 2, Transcranial approach, Optic canal, Cranial aperture, Computed tomography

INTRODUCTION

The cranial aperture (CA) of the optic canal (OC) serves as a passage for structures such as the optic nerve, ophthalmic artery, and sympathetic fibers between the middle cranial fossa and the orbit (2,22). The CA is clinically significant, as compression of the optic nerve commonly occurs at the proximal portion of the OC (17,29,42). This compression may result from two main causes: (a) isolated lesions originating from neurovascular structures within the OC, such as optic nerve sheath meningiomas, and (b) larger

Mehmet Zeki ERDEM : 0000-0003-3263-4633
Abdulmutalip KARAASLANLI : 0009-0005-1046-3484
Abdulaziz YALINKILIC : 0000-0003-2702-5905
Ozkan ARABACI : 0000-0001-7546-8079
Zulkuf AKDEMIR : 0000-0001-7958-7235
Burhan BEGER : 0000-0002-1565-8062
Baris ASLANOGLU : 0000-0003-0623-7730
Turan KOC : 0000-0001-6970-3351
Orhan BEGER : 0000-0002-4932-8758

This work is licensed by "Creative Commons Attribution-NonCommercial-4.0 International (CC)".

lesions extending from the supra- and parasellar regions, such as tuberculum sellae meningiomas (12,17,24,29,35, 38,41,42). In certain cases, limited bone removal around the CA may be adequate for decompression of the OC (17,38,42). Additionally, anatomical information about the proximal segment of the OC—such as its angulation, depth, and dimensions—can assist surgical teams in achieving proper orientation during procedures involving implant placement (14). Therefore, thorough knowledge of CA anatomy is essential for the effective execution of such surgical approaches.

Recent studies have shown that the bony structures of the entire skull base are significantly influenced by Chiari malformation type 1 (CMT1) and type 2 (CMT2) (28,30,34,37). Ozalp et al. compared the CA morphology between CMT1 patients and controls, finding that the position and angulation of the proximal OC were altered in CMT1 (30). Variations in cranial base anatomy—such as the location and angulation of the CA—in individuals with CMT1 or CMT2 may impact the choice of surgical technique, intraoperative orientation, and head positioning during procedures (4,5,28,30-33). However, no studies to date have specifically addressed the anatomical characteristics of the proximal OC, including detailed CA-related descriptions, in patients with CMT2. Therefore, a new investigation focusing on the CA in CMT2 may help determine whether this bony structure exhibits anatomical differences compared to healthy individuals.

The primary aim of this study is to assess the anatomical features of the CA in order to contribute to the existing literature on cranial base morphology in patients with CMT2.

MATERIAL and METHODS

Ethics Statement

This study received ethical approval from the Clinical Research Ethics Committee (approval no: 2024/13-09, dated 20/12/2024).

Study Design

The study population was categorized into two groups: patients with CMT2 and control subjects. These groups were formed based on a review of patient records. The files included details such as admission and discharge dates, presenting complaints, diagnostic procedures, treatment methods, radiological images (MRI, magnetic resonance imaging; CT, computed tomography), and demographic information including age and gender.

Inclusion and Exclusion Criteria

Patients in the CMT2 group presented with herniation of brain structures—including the cerebellar vermis, brainstem, and fourth ventricle—and had a documented history of meningomyelocele. The inclusion criteria for this group were (a) availability of high-quality preoperative MRI and CT images and (b) a confirmed diagnosis of CMT2 based on clinical and radiological evaluations conducted between 2010 and 2024. The exclusion criteria were (a) presence of other types of Chiari malformation, such as CMT1, (b) any cranial base pathology (e.g., tumor), and (c) a history of surgery involving the anterior or middle cranial fossae.

For the control group, inclusion criteria were (a) availability of high-quality MRI and CT images and (b) no known abnormalities (e.g., healthy individuals). Exclusion criteria included (a) presence of any congenital malformation or genetic disorder, (b) any pathological condition such as a tumor, and (c) a history of medical or surgical intervention involving the skull base.

Study Population

The study included CT scans from 40 patients with CMT2, with a mean age of 10.05 ± 4.51 years (range, 6–18 years). This group comprised 16 females (mean age, 10.59 ± 4.63 years) and 24 males (mean age, 9.67 ± 3.47 years), with no significant age difference between genders (p=0.253). Additionally, CT scans from 40 control subjects were analyzed, with a mean age of 10.03 ± 4.81 years (range, 6–18 years). This group included 21 females (mean age, 9.93 ± 4.69 years) and 19 males (mean age, 10.13 ± 3.93 years), also showing no significant age difference between genders (p=0.812).

CT Protocol

Raw imaging data were acquired using a dual-source 128-slice CT scanner (SOMATOM Definition Flash, Siemens Healthineers, Forchheim, Germany). From these datasets, axial, coronal, and sagittal plane images were reconstructed. Morphological details of the anterior clinoid process and optic strut were evaluated using 3D Slicer software (version 5.2.1; https://www.slicer.org/).

Measured Parameters

Eight parameters were measured to evaluate the CA, as summarized in Table I. These included the height (HCA), width (WCA), and surface area (ACA) of the CA, the distances from the CA to the anterior (AB-CA) and lateral (LB-CA) margins of the anterior cranial base, the distance to the midsagittal line (MSL-CA), and the angles of the OC in the axial (APA) and sagittal (SPA) planes (30,40). Axial CT slices were used to measure APA, ACA, AB-CA, LB-CA, and MSL-CA. Coronal slices were used for HCA and WCA measurements, while sagittal slices were used for SPA (Figures 1 and 2).

Statistical Analysis

Comparisons between the CMT2 and control groups, and between male and female subjects, were performed using independent samples t-test. Right–left side comparisons were conducted using paired samples t-tests. The normality of the data, taking into account pediatric developmental stages (late childhood, prepubescence, and postpubescence), was assessed using the Shapiro–Wilk test (40). Statistical analyses were conducted using SPSS software (version 22.0; IBM, Armonk, NY). A p-value of less than 0.05 was considered statistically significant.

RESULTS

In the CMT2 group, the measurements were as follows: HCA

Table I: Definitions and Abbreviations of the Parameters

Parameters	Units	Descriptions
HCA	mm	Vertical diameter of the optic canal's cranial aperture in coronal plane on CT
WCA	mm	Horizontal diameter of the optic canal's cranial aperture in coronal plane on CT
ACA	mm^2	Surface area of the optic canal's cranial aperture in coronal plane on CT
AB-CA	mm	Distance between the optic canal's cranial aperture (the frontmost point) and the anterior boundary of the anterior skull base in axial plane on CT
LB-CA	mm	Distance between the optic canal's cranial aperture (the most lateral point) and the lateral boundary of the anterior skull base in axial plane on CT
MSL-CA	mm	Distance between the optic canal's cranial aperture (the most medial point) and the midsagittal line in axial plane on CT
APA	degree	Angle between the optic canal and the sagittal horizontal line (i.e., the midline axis) in axial plane on CT
SPA	degree	Angle between the optic canal and the sagittal horizontal line (i.e., the line parallel to the ground) in sagittal plane on CT

CT: *Computed tomography.* ***HCA:*** *The height of the cranial aperture,* ***WCA:*** *The width of the cranial aperture,* ***ACA:*** *The surface area of the cranial aperture,* ***AB-CA:*** *The distance from the cranial aperture to the anterior margin of the anterior cranial base,* ***LB-CA:*** *The distance from the cranial aperture to the lateral margin of the anterior cranial base,* ***MSL-CA:*** *The distance from the cranial aperture to the midsagittal line,* ***APA:*** *The angle of the optic canal in the axial plane,* ***SPA:*** *The angle of the optic canal in the sagittal plane.*

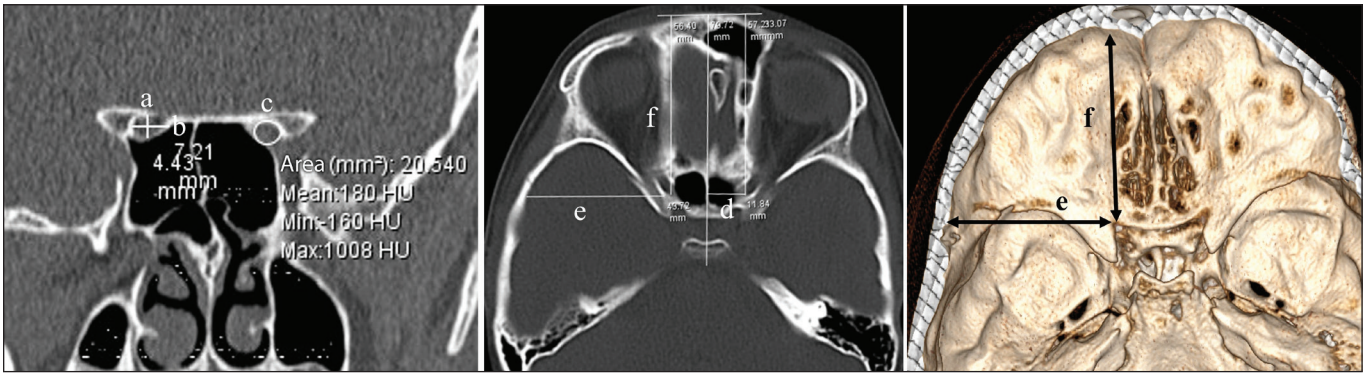

Figure 1: Measured parameters related to the size and position of the cranial aperture (CA). **a)** the height of the CA (HCA), **b)** the width of the CA (WCA), **c)** the surface area of the CA (ACA), **d)** the distance from the CA to the midsagittal line (MSL-CA), **e)** the distance from the CA to the lateral margin of the anterior cranial base (LB-CA), and **f)** the distance from the CA to the anterior margin of the anterior cranial base (AB-CA). A line was drawn parallel to the midsagittal line, starting from the frontmost point of the CA and ending at the point where the squamous and orbital parts of the frontal bone meet on the inner surface of the anterior boundary of the anterior skull base. This line was used to measure AB-CA, the distance from the CA to the anterior boundary of the anterior fossa, on the axial CT plane. Additionally, a perpendicular line was drawn from the most lateral point of the CA to the point on the inner surface of the lateral boundary of the anterior skull base, this line was used to measure LB-CA, the distance from the CA to the lateral boundary of the anterior fossa, on the axial CT plane.

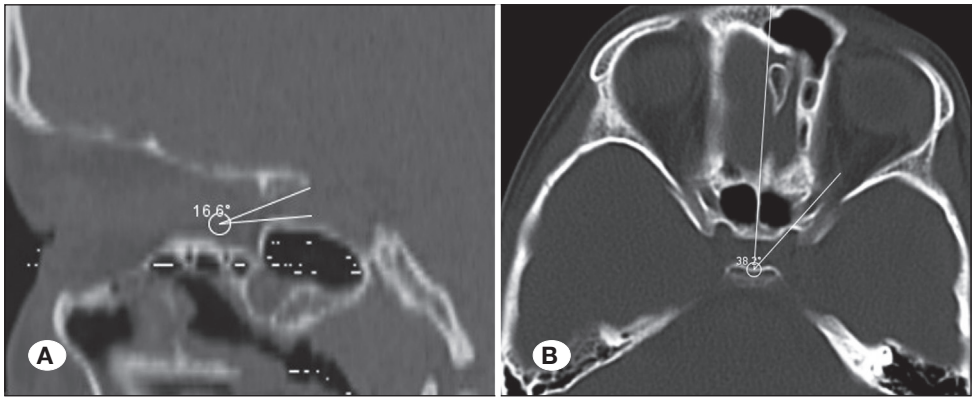

Figure 2: Parameters related to the angulation of the optic canal (OC). **A)** the angle of the optic canal in the sagittal plane (SPA), and **B)** the angle of the optic canal in the axial plane (APA).

Table II: Comparison of CMT2 and Controls (the Independent Test)

Parameters	CMT2 (n=80)	Control (n=80)	p-value
HCA (mm)	3.64 ± 0.81	4.22 ± 0.60	**<0.001**
WCA (mm)	3.08 ± 0.87	4.54 ± 1.04	**<0.001**
ACA (mm^2)	7.58 ± 2.84	12.81 ± 3.80	**<0.001**
AB-CA (mm)	44.99 ± 7.69	52.73 ± 6.71	**<0.001**
LB-CA (mm)	29.17 ± 5.03	35.86 ± 4.33	**<0.001**
MSL-CA (mm)	7.07 ± 2.44	10.21 ± 2.21	**<0.001**
APA (°)	30.64 ± 6.03	35.96 ± 3.23	**<0.001**
SPA (°)	24.31 ± 5.09	28.64 ± 4.34	**<0.001**

N: *Numbers of sides.* ***CMT2:*** *Chiari malformation type 2,* ***HCA:*** *The height of the cranial aperture,* ***WCA:*** *The width of the cranial aperture,* ***ACA:*** *The surface area of the cranial aperture,* ***AB-CA:*** *The distance from the cranial aperture to the anterior margin of the anterior cranial base,* ***LB-CA:*** *The distance from the cranial aperture to the lateral margin of the anterior cranial base,* ***MSL-CA:*** *The distance from the cranial aperture to the midsagittal line,* ***APA:*** *The angle of the optic canal in the axial plane,* ***SPA:*** *The angle of the optic canal in the sagittal plane.*

3.64 ± 0.81 mm, WCA 3.08 ± 0.87 mm, ACA 7.58 ± 2.84 mm^2, AB-CA 44.99 ± 7.69 mm, LB-CA 29.17 ± 5.03 mm, MSL-CA 7.07 ± 2.44 mm, APA 30.64° ± 6.03°, and SPA 24.31° ± 5.09°. In the control group, the corresponding values were HCA 4.22 ± 0.60 mm, WCA 4.54 ± 1.04 mm, ACA 12.81 ± 3.80 mm^2, AB-CA 52.73 ± 6.71 mm, LB-CA 35.86 ± 4.33 mm, MSL-CA 10.21 ± 2.21 mm, APA 35.96° ± 3.23°, and SPA 28.64° ± 4.34°.

All measured parameters (HCA, WCA, ACA, AB-CA, LB-CA, MSL-CA, APA, and SPA) were significantly smaller in the CMT2 group compared to the controls (p<0.001) (Table II).

Among CMT2 patients, females had a significantly smaller LB-CA than males (p=0.034). In the control group, females had smaller WCA (p=0.038), AB-CA (p<0.001), and LB-CA (p=0.015) than males. No statistically significant differences were found between the right and left sides in either group (p>0.05) (Table III).

DISCUSSION

CMT2 is a congenital anomaly with an estimated incidence of 0.04%, and it shows no gender preference (19,21). It is primarily attributed to a neural tube defect (26), which disrupts cerebrospinal fluid flow and results in the downward displace-

Table III: Gender (The Independent Test) and Side (the Paired Test) Comparisons for CMT2 and Controls

	Parameters	Female (n=32)	Male (n=48)	p-value	Right (n=40)	Left (n=40)	p-value
CMT2	HCA (mm)	3.60 ± 0.97	3.67 ± 0.70	0.731	3.72 ± 0.84	3.56 ± 0.79	0.390
	WCA (mm)	3.04 ± 0.78	3.11 ± 0.94	0.740	3.10 ± 0.81	3.05 ± 0.94	0.805
	ACA (mm^2)	7.29 ± 2.74	7.77 ± 2.92	0.465	7.32 ± 2.31	7.83 ± 3.30	0.428
	AB-CA (mm)	43.98 ± 8.81	45.67 ± 6.86	0.339	45.06 ± 7.57	44.93 ± 7.91	0.941
	LB-CA (mm)	27.72 ± 5.50	30.14 ± 4.48	0.034	30.38 ± 5.16	27.97 ± 4.65	0.052
	MSL-CA (mm)	7.07 ± 2.22	7.07 ± 2.60	0.999	7.17 ± 2.50	6.97 ± 2.41	0.727
	APA (°)	30.23 ± 5.12	30.91 ± 6.60	0.627	30.44 ± 5.63	30.84 ± 6.46	0.770
	SPA (°)	24.18 ± 5.43	24.40 ± 4.91	0.851	24.46 ± 5.20	24.17 ± 5.05	0.799
	Parameters	**Female (n=42)**	**Male (n=38)**	**p-value**	**Right (n=40)**	**Left (n=40)**	**p-value**
Control	HCA (mm)	4.20 ± 0.63	4.25 ± 0.58	0.674	4.28 ± 0.59	4.17 ± 0.62	0.398
	WCA (mm)	4.31 ± 0.84	4.79 ± 1.18	0.038	4.47 ± 0.94	4.60 ± 1.14	0.578
	ACA (mm^2)	12.27 ± 3.29	13.41 ± 4.26	0.180	12.66 ± 3.40	12.96 ± 4.20	0.724
	AB-CA (mm)	49.42 ± 5.10	56.38 ± 6.42	<0.001	52.74 ± 6.64	52.72 ± 6.88	0.988
	LB-CA (mm)	34.75 ± 3.94	37.09 ± 4.45	0.015	37.43 ± 3.61	34.30 ± 4.46	0.061
	MSL-CA (mm)	9.83 ± 1.92	10.64 ± 2.45	0.100	10.15 ± 2.32	10.28 ± 2.12	0.786
	APA (°)	36.06 ± 2.76	35.84 ± 3.71	0.756	34.81 ± 3.30	37.11 ± 2.74	0.082
	SPA (°)	29.43 ± 4.48	27.77 ± 4.05	0.088	28.79 ± 4.24	28.50 ± 4.48	0.761

N: *Numbers of sides.* ***CMT2:*** *Chiari malformation type 2,* ***HCA:*** *The height of the cranial aperture,* ***WCA:*** *The width of the cranial aperture,* ***ACA:*** *The surface area of the cranial aperture,* ***AB-CA:*** *The distance from the cranial aperture to the anterior margin of the anterior cranial base,* ***LB-CA:*** *The distance from the cranial aperture to the lateral margin of the anterior cranial base,* ***MSL-CA:*** *The distance from the cranial aperture to the midsagittal line,* ***APA:*** *The angle of the optic canal in the axial plane,* ***SPA:*** *The angle of the optic canal in the sagittal plane.*

ment of brain tissue into the spinal canal (19,21,26). CMT2 is characterized by (a) the presence of a myelomeningocele, (b) a reduced posterior fossa volume, and (c) downward displacement of the fourth ventricle, brainstem, and cerebellum (13,25). This condition may lead to symptoms such as facial muscle weakness, difficulty swallowing, nystagmus, musculoskeletal deformities, and selective sensory loss (19,21). Although CMT2 is generally regarded as a posterior fossa malformation, it has been suggested that bony structures in other cranial fossae may also be affected (34). For example, compared to healthy individuals, patients with CMT2 have been found to have a shallower sella, an apparently taller but non-pathological pituitary gland, a shortened dorsum sellae, and an elongated tuberculum sellae (34). Patel et al. noted that such alterations could lead to misinterpretations during imaging, such as mistaking a normally sized gland for an enlarged one due to the reduced sella depth on MRI (34). Based on these findings, we suggest that further studies are needed to evaluate whether CMT2 also alters the morphology of structures like the CA located in the anterior and middle cranial fossae.

In patients with Chiari malformations, such as CMT1, optic nerve compression can be identified by physicians due to conditions like osteopetrosis, which can lead to narrowing of the OC and thickening of the optic strut (3,16,27). For example, Medsinge et al. used a transcaruncular endoscopic approach to perform OC decompression in a 6-month-old girl with CMT1 (27). Surgical management of OC compression is crucial for the surgical team (6,17,24,29,38,41,42). In some cases, complete removal of the OC walls, including the optic strut and anterior clinoid process, may be required for 270° decompression (6), while in others, removing only the proximal part of the OC may be enough for decompression (17,38,42). The location, angulation, and size of anatomical structures in the supra- and parasellar regions can influence the choice of surgical approach (8-10,17,18). For example, some lesions can distort the OC's bone structure, affecting the optic nerve's position, and in these cases, surgeons may choose to follow the normal path of the optic nerve to avoid iatrogenic injury (18). Detailed knowledge of the CA anatomy is important to minimize morbidity and mortality (7,15,17,18,23,40). Our novel morphometric data could help physicians determine whether the OCs in CMT2 patients differ from those in healthy individuals and assist in selecting appropriate surgical techniques for CMT2 cases.

In CMT2, the measurements for HCA, WCA, ACA, AB-CA, LB-CA, MSL-CA, APA, and SPA were found to be 3.64 ± 0.81 mm, 3.08 ± 0.87 mm, 7.58 ± 2.84 mm^2, 44.99 ± 7.69 mm, 29.17 ± 5.03 mm, 7.07 ± 2.44 mm, 30.64° ± 6.03°, and 24.31° ± 5.09°, respectively. In the control group, the measurements were 4.22 ± 0.60 mm, 4.54 ± 1.04 mm, 12.81 ± 3.80 mm^2, 52.73 ± 6.71 mm, 35.86 ± 4.33 mm, 10.21 ± 2.21 mm, 35.96° ± 3.23°, and 28.64° ± 4.34°, respectively. The results showed that CMT2 patients had significantly smaller HCA, WCA, ACA, AB-CA, LB-CA, MSL-CA, APA, and SPA compared to the controls ($p<0.001$). These smaller measurements suggest that patients with CMT2 likely have a smaller skull base compared to controls. Ozalp et al. reported measurements in CMT1 (30), where HCA was 3.69 ± 0.69 mm, WCA was 5.15 ± 0.96 mm, AB-CA was 52.82 ± 6.14 mm, LB-CA was 37.50 ± 4.21 mm, MSL-CA was 7.64 ± 1.64 mm, APA was 34.42° ± 5.29°, and SPA was 15.04° ± 3.80°, and in controls, HCA was 3.75 ± 1.18 mm, WCA was 5.30 ± 1.25 mm, AB-CA was 57.41 ± 7.40 mm, LB-CA was 39.43 ± 4.49 mm, MSL-CA was 7.67 ± 1.91 mm, APA was 31.80° ± 4.89°, and SPA was 14.97° ± 3.28°. They found that CMT1 patients had smaller AB-CA ($p<0.001$) and LB-CA ($p=0.003$) compared to controls, but a larger APA ($p=0.006$) (30). They suggested that AB-CA and LB-CA represent the length and width of the anterior fossa, respectively, and concluded that CMT1 patients had a shorter and narrower anterior fossa than normal individuals (30). Based on this interpretation, we propose that CMT2 patients also have a shorter and narrower anterior fossa due to their smaller AB-CA and LB-CA measurements.

The existing literature indicates that the mean values of the parameters vary widely (1,7,30,40). In normal adults, the mean values range from 4.59–7.38 mm for WCA, 3.60–5.17 mm for HCA, 4.45–19.36 mm^2 for ACA, 29.56°–45.32° for APA, 7.57°–18.20° for SPA, 5.77–7.64 mm for MSL-CA, 41–42.55 mm for LB-CA, and 44.38–64.97 mm for AB-CA (1,30,40). In normal children aged 1–18 years, the values for HCA, WCA, ACA, AB-CA, LB-CA, MSL-CA, APA, and SPA were found to be 4.35 ± 0.64 mm, 6.12 ± 0.84 mm, 17.53 ± 2.80 mm^2, 54.04 ± 5.23 mm, 42.55 ± 3.28 mm, 7.17 ± 1.48 mm, 39.28° ± 5.13°, and 16.01° ± 6.76°, respectively (40). The HCA and AB-CA values in our controls were similar to those in this pediatric study. However, compared to the values reported by Ten et al., our controls had smaller WCA, ACA, LB-CA, and APA values, but larger MSL-CA and SPA values (40). Ten et al. also noted that the size of the CA correlated with age and that the APA and LB-CA did not change significantly after the ages of 3 and 6, respectively. AB-CA remained consistent from the age of 14, while HCA, WCA, SPA, and MSL-CA stabilized from the age of 10 (40). In fetuses aged 16–28 weeks of gestation, HCA, WCA, and ACA were measured as 1.58 ± 0.36 mm, 1.83 ± 0.59 mm, and 2.40 ± 1.02 mm^2, respectively (7), with these parameters increasing as fetal age progressed (7). The pediatric values in our controls were significantly higher than these fetal measurements. Thus, age is a key factor influencing the differences in mean values observed in earlier studies (7,14,40). Another factor could be the selection of different landmarks, particularly for distance measurements (AB-CA, MSL-CA, LB-CA) (14,40). Methodological differences may also contribute to variations (11,20). Berlis et al. found not difference between CT and caliper measurements, while Kalthur et al. reported that CT values were significantly smaller than caliper values (11,20). For ACA, differences in calculation methods may explain discrepancies in mean values (36,39). The mean value calculated by Radunovic et al. using the formula (width x height x π) was 19.36 ± 1.87 mm^2 (36), which was higher than the mean value obtained using software by Tao et al. (4.45 ± 0.46 mm^2) (39).

This study has several limitations. First, the sample sizes for both CMT2 and control groups were small. Larger studies with more participants could provide a clearer understanding of CA anatomy in CMT2 patients. Second, we focused on pediatric

patients with CMT2, as most CMT2 patients admitted to our hospital were children. Previous studies have indicated that combining adult and pediatric data may lead to inaccurate conclusions due to differences in skull base morphology. Therefore, future research including adult patients may offer valuable insights into CA morphology in CMT2 cases. Third, we examined CA morphology only in CMT2 patients and found significant differences compared to controls. Building on the work of Ozalp et al., who identified notable differences in CA anatomy between CMT1 patients and controls, we believe that further studies involving both CMT1 and CMT2 patients would be beneficial for clinicians to better understand skull base development in different Chiari malformations (30).

CONCLUSION

Patients with CMT2 exhibited significantly smaller HCA, WCA, ACA, AB-CA, LB-CA, MSL-CA, APA, and SPA compared to controls. Specifically, measurements of depth and angle may be crucial for surgeons to safely perform procedures such as OC decompression in CMT2 patients.

Declarations

Funding: This research did not receive any specific grant from funding agencies in the public, commercial, or not-for-profit sectors.

Availability of data and materials: The datasets generated and/or analyzed during the current study are available from the corresponding author by reasonable request.

Disclosure: The authors declare no competing interests.

AUTHORSHIP CONTRIBUTION

Study conception and design: MZE, AK, AY, BB
Data collection: OA, BA, AK, ZA
Analysis and interpretation of results: TK, OB, AK, OA
Draft manuscript preparation: AK, OB, TK
Critical revision of the article: AK, OB, OA
All authors (AK, MZE, AY, OA, ZA, BB, BA, TK, OB) reviewed the results and approved the final version of the manuscript.

REFERENCES

1. Adanir SS, Baksi YE, Beger O, Bahsi I, Kervancioglu P, Yalcin ED, Orhan M: Evaluation of the cranial Aperture of the optic canal on cone-beam computed tomography images and its clinical Implications for the transcranial approaches. J Craniofac Surg 33:1909-1913, 2022. https://doi.org/10.1097/SCS.0000000000008577
2. Adanir SS, Beger O, Bahsi I: A terminological confusion: Optic foramen or canal? Surg Radiol Anat 43:577-578, 2021. https://doi.org/10.1007/s00276-021-02679-9
3. Alagappan A, Satpathy AK, Sahoo B, Nayak MK: Osteopetrosis with Arnold Chiari malformation type I. BMJ Case Rep 16:e254559, 2023. doi: 10.1136/bcr-2023-254559. https://doi.org/10.1136/bcr-2023-254559
4. Alpergin BC, Eroglu U, Yakar F, Karadagoglu U, Ozpiskin OM, Gokalp E, Gurses ME, Cetin M, Beger O: Radioanatomical assessment of the sphenoid ridge in Chiari type I malformation. Turk Neurosurg, 2024 (Online ahead of print). https://doi.org/10.5137/1019-5149.JTN.46851-24.3
5. Alpergin BC, Eroglu U, Zaimoglu M, Kilinc MC, Ozpiskin OM, Erdin E, Beger O: Topographic anatomy and pneumatization of the posterior clinoid process in Chiari type I malformation. World Neurosurg 185:e767-e773, 2024. https://doi.org/10.1016/j.wneu.2024.02.130
6. Beer-Furlan A, Evins AI, Rigante L, Burrell JC, Anichini G, Stieg PE, Bernardo A: Endoscopic extradural anterior clinoidectomy and optic nerve decompression through a pterional port. J Clin Neurosci 21:836-840, 2014. https://doi.org/10.1016/j.jocn.2013.10.006
7. Beger O: Assessment of the optic foramen shape and size in human fetuses. J Craniofac Surg 31:2021-2024, 2020. https://doi.org/10.1097/SCS.0000000000006610
8. Beger O, Bahsi I: Chiasmatic ridge: Incidence, classification, and clinical implications. J Craniofac Surg 32:1910-1912, 2021. https://doi.org/10.1097/SCS.0000000000007291
9. Beger O, Taghipour P, Cakir S, Hamzaoglu V, Ozalp H, Kara E, Vayisoglu Y, Dagtekin O, Dagtekin A, Bagdatoglu C, Ozturk AH, Talas DU: Fetal anatomy of the optic strut and prechiasmatic sulcus with a clinical perspective. World Neurosurg 136:e625-e634, 2020. https://doi.org/10.1016/j.wneu.2020.01.125
10. Beger O, Ten B, Balci Y, Cakir S, Ozalp H, Hamzaoglu V, Vayisoglu Y, Dagtekin A, Bagdatoglu C, Talas DU: A computed tomography study of the prechiasmatic sulcus anatomy in children. World Neurosurg 141:e118-e132, 2020. https://doi.org/10.1016/j.wneu.2020.05.023
11. Berlis A, Putz R, Schumacher M: Direct and CT measurements of canals and foramina of the skull base. Brit J Radiol 65:653-661, 1992. https://doi.org/10.1259/0007-1285-65-776-653
12. Caporlingua A, Prior A, Cavagnaro MJ, Winston G, Oliveira DLC, Sadwhani SD, Arias GA, Schwalb JN, Akhbari M, Evins AI, Bernardo A: The intracranial and intracanalicular optic nerve as seen through different surgical windows: Endoscopic versus transcranial. World Neurosurg 124:522-538, 2019. https://doi.org/10.1016/j.wneu.2019.01.122
13. Cesmebasi A, Loukas M, Hogan E, Kralovic S, Tubbs RS, Cohen-Gadol AA: The Chiari malformations: A review with emphasis on anatomical traits. Clin Anat 28:184-194, 2015. https://doi.org/10.1002/ca.22442
14. Chang JT, Morrison CS, Styczynski JR, Mehan W, Sullivan SR, Taylor HO: Pediatric orbital depth and growth: A radiographic analysis. J Craniofac Surg 26:1988-1991, 2015. https://doi.org/10.1097/SCS.0000000000001974
15. Gagliardi F, Donofrio CA, Spina A, Bailo M, Gragnaniello C, Gallotti AL, Elbabaa SK, Caputy AJ, Mortini P: Endoscope-assisted transmaxillosphenoidal approach to the sellar and parasellar regions: An anatomic study. World Neurosurg 95:246-252, 2016. https://doi.org/10.1016/j.wneu.2016.08.034
16. Goodwin D, Halvorson AR: Chiari I malformation presenting as downbeat nystagmus: Clinical presentation, diagnosis, and management. Optometry 83:80-86, 2012.

17. Guler TM, Yılmazlar S, Ozgun G: Anatomical aspects of optic nerve decompression in transcranial and transsphenoidal approach. J Craniomaxillofac 47:561-569, 2019. https://doi.org/10.1016/j.jcms.2019.01.027
18. Guthikonda B, Tobler WD Jr, Froelich SC, Leach JL, Zimmer LA, Theodosopoulos PV, Tew JM Jr, Keller JT: Anatomic study of the prechiasmatic sulcus and its surgical implications. Clin Anat 23:622-628, 2010. https://doi.org/10.1002/ca.21002
19. Hidalgo JA, Tork CA, Varacallo M: Arnold-chiari malformation. In: StatPearls [Internet]. Treasure Island (FL): StatPearls Publishing, 2024.
20. Kalthur S, Periyasamy R, Kumar S, Gupta C, D'souza AS: A morphometric evaluation of the optic canal: Comparative study between computerized tomographic study and direct anatomic study. Saudi J Med Med Sci 3:204-208, 2015. https://doi.org/10.4103/1658-631X.161997
21. Kuhn J, Weisbrod LJ, Emmady PD: Chiari Malformation Type 2. In: StatPearls (Internet). Treasure Island (FL): StatPearls Publishing, 2024.
22. Kumar A, Tripathi A, Jain S, Khare S, Kaushik RK, Kausar H, Arora S: Anatomical and morphometric study of optic foramen in North Indian Population. Natl J Clin Anat 8:053-056, 2019. https://doi.org/10.1055/s-0039-1689079
23. Locatelli M, Di Cristofori A, Draghi R, Bertani G, Guastella C, Pignataro L, Mantovani G, Rampini P, Carrabba G: Is complex sphenoidal sinus anatomy a contraindication to a transsphenoidal approach for resection of sellar lesions? Case series and review of the literature. World Neurosurg 100:173-179, 2017. https://doi.org/10.1016/j.wneu.2016.12.123
24. Maurer J, Hinni M, Mann W, Pfeiffer N: Optic nerve decompression in trauma and tumor patients. Eur Arch Otorhinolaryngol 256:341-345, 1999. https://doi.org/10.1007/s004050050160
25. McLone DG, Dias MS: The Chiari II malformation: Cause and impact. Childs Nerv Syst 19:540-550, 2023. https://doi.org/10.1007/s00381-003-0792-3
26. McLone DG, Knepper PA: The cause of Chiari II malformation: A unified theory. Pediatr Neurosci 15:1-12, 1989. https://doi.org/10.1159/000120432
27. Medsinge A, Sylvester C, Tyler-Kabara E, Stefko ST: Bilateral endoscopic optic nerve decompression in an infant with osteopetrosis. J AAPOS 23:40-42, 2019. https://doi.org/10.1016/j.jaapos.2018.05.012
28. Nwotchouang BST, Eppelheimer MS, Bishop P, Biswas D, Andronowski JM, Bapuraj JR, Frim D, Labuda R, Amini R, Loth F: Three-dimensional CT morphometric image analysis of the clivus and sphenoid sinus in Chiari malformation type I. Ann Biomed Eng 47:2284-2295, 2019. https://doi.org/10.1007/s10439-019-02301-5
29. Onofrey CB, Tse DT, Johnson TE, Neff AG, Dubovy S, Buck BE, Casiano R: Optic canal decompression: A cadaveric study of the effects of surgery. Ophthalmic Plast Reconstr Surg 23:261-266, 2007. https://doi.org/10.1097/IOP.0b013e3180cac220
30. Ozalp H, Ozgural O, Alpergin BC, Inceoglu A, Ozalp S, Armagan E, Ucar H, Beger O: Analysis of the cranial aperture of the optic canal in patients with Chiari Type-I malformation. Turk Neurosurg 34:1081-1092, 2024. https://doi.org/10.5137/1019-5149.JTN.45482-23.2
31. Ozalp H, Ozgural O, Alpergin BC, Inceoglu A, Ozalp S, Armagan E, Ucar H, Beger O: Analysis of the prechiasmatic sulcus in Chiari malformation type I. World Neurosurg 175:e1149-e1157, 2023. https://doi.org/10.1016/j.wneu.2023.04.083
32. Ozalp H, Ozgural O, Alpergin BC, Inceoglu A, Ozalp S, Armagan E, Ucar H, Beger O: Assessment of the anterior clinoid process and optic strut in Chiari malformation type I: A computed tomography study. J Neurol Surg B Skull Base 85:302-312, 2023. https://doi.org/10.1055/s-0043-57248
33. Ozalp H, Ozgural O, Alpergin BC, Inceoglu A, Ozalp S, Armagan E, Ucar H, Beger O: Evaluation of the sella morphology in Chiari malformation type I. Turk Neurosurg 35:171-181, 2025. https://doi.org/10.5137/1019-5149.JTN.45939-23.3
34. Patel D, Saindane A, Oyesiku N, Hu R: Variant sella morphology and pituitary gland height in adult patients with Chiari II malformation: Potential pitfall in MRI evaluation. Clin Imaging 64:24-28, 2020. https://doi.org/10.1016/j.clinimag.2020.02.014
35. Puzzilli F, Ruggeri A, Mastronardi L, Agrillo A, Ferrante L: Anterior clinoidal meningiomas: Report of a series of 33 patients operated on through the pterional approach. Neuro Oncol 1:188-195, 1999. https://doi.org/10.1093/neuonc/1.3.188
36. Radunovic M, Vukcevic B, Radojevic N, Vukcevic N, Popovic N, Vuksanovic-Bozaric A: Morphometric characteristics of the optic canal and the optic nerve. Folia Morphol (Warsz) 78:39-46, 2019. https://doi.org/10.5603/FM.a2018.0065
37. Sgouros S, Kountouri M, Natarajan K: Skull base growth in children with Chiari malformation Type I. J Neurosurg 107:188-192, 2007. https://doi.org/10.3171/PED-07/09/188
38. Taha AN, Erkmen K, Dunn IF, Pravdenkova S, Al-Mefty O: Meningiomas involving the optic canal: Pattern of involvement and implications for surgical technique. Neurosurg Focus 30:E12, 2011. https://doi.org/10.3171/2011.2.FOCUS1118
39. Tao H, Ma Z, Dai P, Jiang L: Computer-aided three-dimensional reconstruction and measurement of the optic canal and intracanalicular structures. Laryngoscope 109:1499-1502, 1999. https://doi.org/10.1097/00005537-199909000-00026
40. Ten B, Beger O, Esen K, Adanir SS, Hamzaoglu EC, Cicek F, Taghipour P, Kara E, Vayisoglu Y, Talas DU: Anatomic features of the cranial aperture of the optic canal in children: A radiologic study. Surg Radiol Anat 43:187-199, 2021. https://doi.org/10.1007/s00276-020-02604-6
41. Yang Y, Wang H, Shao Y, Wei Z, Zhu S, Wang J: Extradural anterior clinoidectomy as an alternative approach for optic nerve decompression: Anatomic study and clinical experience. Neurosurgery 59:ONS253-62; discussion ONS262, 2006. https://doi.org/10.1227/01.NEU.0000236122.28434.13
42. Yilmazlar S, Saraydaroglu O, Korfali E: Anatomical aspects in the transsphenoidal-transethmoidal approach to the optic canal: An anatomic-cadaveric study. J Craniomaxillofac Surg 40:e198-e205, 2012. https://doi.org/10.1016/j.jcms.2011.10.008